ISSN 1995-0780, Nanotechnologies in Russia, 2020, Vol. 15, Nos. 3–6, pp. 356–362. © Pleiades Publishing, Ltd., 2020.
Russian Text © The Author(s), 2020, published in Rossiiskie Nanotekhnologii, 2020, Vol. 15, No. 3, pp. 368–375.

DEVICES AND PRODUCTS BASED ON NANOMATERIALS AND NANOTECHNOLOGIES

Formation and Electrochemical Activity of Nanostructured Anodes of Solid Oxide Fuel Cells in Hydrogen-Containing Atmospheres

E. V. Tsipis[a,*], I. N. Burmistrov[a,b], D. A. Agarkov[a,b], D. V. Matveev[a,b], V. V. Kharton[a], and S. I. Bredikhin[a,b]

[a] *Institute of Solid State Physics, Russian Academy of Sciences, Chernogolovka, Moscow oblast, Russia*
[b] *Moscow Institute of Physics and Technology (National Research University), Dolgoprudny, Moscow oblast, Russia*
**e-mail: tsipis@issp.ac.ru*

Received June 9, 2020; revised June 9, 2020; accepted July 19, 2020

Abstract—A comparative analysis of the features of the formation, morphology, and electrochemical activity of composite anodes of solid oxide fuel cells was performed using nanosized particles of NiO and $Ce_{0.8}Gd_{0.2}O_{2-\delta}$. The direct introduction of NiO nanoparticles into cermet composition leads to technological problems during screen printing of electrode layers associated with the oxidation of organic components of electrode pastes with oxygen, which is desorbed from the NiO surface. Such problems can be solved by preheating treatment of NiO. However, this treatment and subsequent firing of the anodes leads to an increase in the particle size to submicron. An increase in electrochemical activity can be achieved by impregnating the anodes with the formation of nanosized catalytically active particles on their surface.

DOI: 10.1134/S1995078020030143

INTRODUCTION

Technologies for creating power plants based on solid oxide fuel cells (SOFCs) are among the most promising for the future energy industry [1–5]. The efficiency of a single SOFC is fundamentally dependent on the electrochemical activity of the electrodes. Despite the well-known problems associated with the deposition of carbon and the enlargement of Ni particles during long-term operation, cermets containing metallic Ni and stabilized zirconia are the most widely used SOFC anode materials [1–7]. The electrochemical activity of SOFC composite electrodes is mainly determined by the three-phase boundary between the electronic conductor, solid electrolyte, and the gas phase [8, 9]. Other factors affecting the electrochemical activity of electrodes are the specific surface area, porosity, and distribution of electron and ion-conducting components, which determine the kinetics of sorption processes, diffusion of gaseous fuel, and transport processes in the solid phase, respectively. One of the important approaches to optimizing the morphology of the anode layer relates to a decrease in the particle size in the initial powders ([6, 7, 10] and the literature cited therein). On the other hand, a significant reduction in the particle size of components can lead to dramatic changes in material properties and electrode behavior. It is assumed that factors such as the tendency to agglomeration, the presence of modified surface layers, and the rapidity of microstructural changes under the operating conditions of SOFCs should determine the procedure for making the electrode and affect the behavior of the anode layer.

The aim of this work is to study the features of the formation of SOFC anode layers fabricated using nanostructured components and the electrochemical activity of such anodes.

EXPERIMENTAL

Commercially available nanosized nickel(II) oxide powder (99.8% purity, Sigma-Aldrich, United States) was used as a model starting reagent for these studies. To optimize the pretreatment conditions, a series of NiO samples were annealed in air at 300, 500, 700, 900, 1000, and 1100°C for 1 h. To form functional anodic composite layers, NiO powders were mixed with 10Sc1CeSZ submicron powder (10 mol % Sc_2O_3- and 1 mol % CeO_2-stabilized ZrO_2, DKKK, Japan). The mass ratio of NiO : 10Sc1CeSZ in the functional electrode layer deposited between the solid electrolyte membrane and the current collector layers was 40 : 60%. Screen printing pastes were prepared by mixing the powders with V-006A binder (Heraeus, Germany) and applied using an Ekra Mat S45 screen printing machine (Asys Group, Germany).

Another experimental approach was used to fabricate three-component anodes containing catalytically

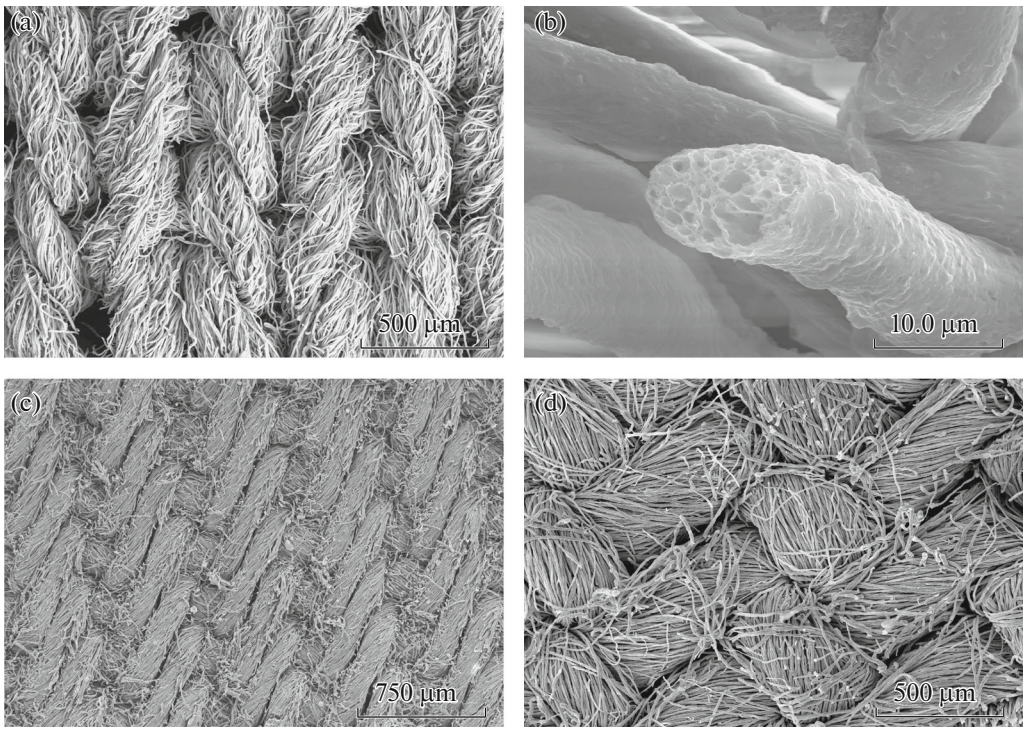

Fig. 1. Morphology of (a, b) GDC20, (c) Ni–GDC20, and (d) Cu–GDC20 powders obtained by the cellulose-precursor method after precursor firing.

active $Ce_{0.8}Gd_{0.2}O_{2-\delta}$ (GDC20). In this case, the nanosized GDC20 powder was synthesized by the cellulose precursor technique [11]. The NiO used to make cermet was obtained by the thermal decomposition of $Ni(NO_3)_2 \cdot 6H_2O$. The third component was a commercial zirconia powder stabilized with 8 mol % yttrium oxide (8YSZ, Tosoh, Japan). The mass ratio of Ni : 8YSZ : GDC20 in cermet after reduction was 50 : 30 : 20%. The anode layers were deposited on a solid electrolyte of lanthanum gallate doped with strontium and magnesium (LSGM), by screen printing. Cermets with compositions of Ni : GDC20 at 25 : 75 wt % or 50 : 50 mol % and of Cu : GDC20 at 27 : 73 wt % or 50 : 50 mol % were also synthesized by the cellulose-precursor method. In this case, oxide fibers retain the texture of the initial cellulose precursor (Fig. 1) and are transformed into homogeneous nanocrystalline powders by light mechanical action (Figs. 2a–2c). Anode layer annealing temperatures were 1250°C for Ni–8YSZ–GDC20 and Ni–GDC20 and 1000°C for Cu-containing cermet.

The crystal structure of powder samples was analyzed by X-ray diffraction analysis (XRD) on a Siemens D-500-Braun diffractometer (radiation CuK_α). The particle size and features of the microstructure of the samples were investigated by transmission (JEOL-100 CXII, accelerating voltage 100 kV), high-resolution (JEOL-2100, accelerating voltage 200 kV), and scanning (Supra 50VP, CarlZeiss) electron microscopy (TEM/SAM). The determination of the chemical composition was carried out using energy dispersive X-ray spectroscopy (EDX). The quality of the applied layers was also evaluated using optical microscopy on an Olympus BX51 (Japan) equipped with a 9.1 MP ToupCam CCD camera. For thermogravimetric analysis (TGA) Setaram Setsys EVO 16 and Netzsch STA 409C Luxx (Germany) devices were used with constant heating at a rate of 2 K/min. The latest analyzer, equipped with a QMS 403C Aeolos quadrupole mass spectrometer, provides simultaneous measurement of TGA signals and differential scanning calorimetry (DSC) in combination with a gas evolution analysis. The experimental techniques and equipment used for measuring the anode overpotential by the three-electrode method, impedance spectroscopy, and studying the current-voltage characteristics of model SOFCs are described in [12–15].

RESULTS AND DISCUSSION

XRD results showed that the initial nanosized NiO powder is single-phase with a pseudocubic lattice parameter equal to 4.178 (2) Å. As expected, at atmospheric oxygen pressure, this phase remains stable over the entire temperature range studied in this work. The average crystallite size in the initial powder, calculated using the Scherrer equation, is 13 nm. This estimate was confirmed by statistical analysis of TEM images (Fig. 3), which showed that the maximum fraction of

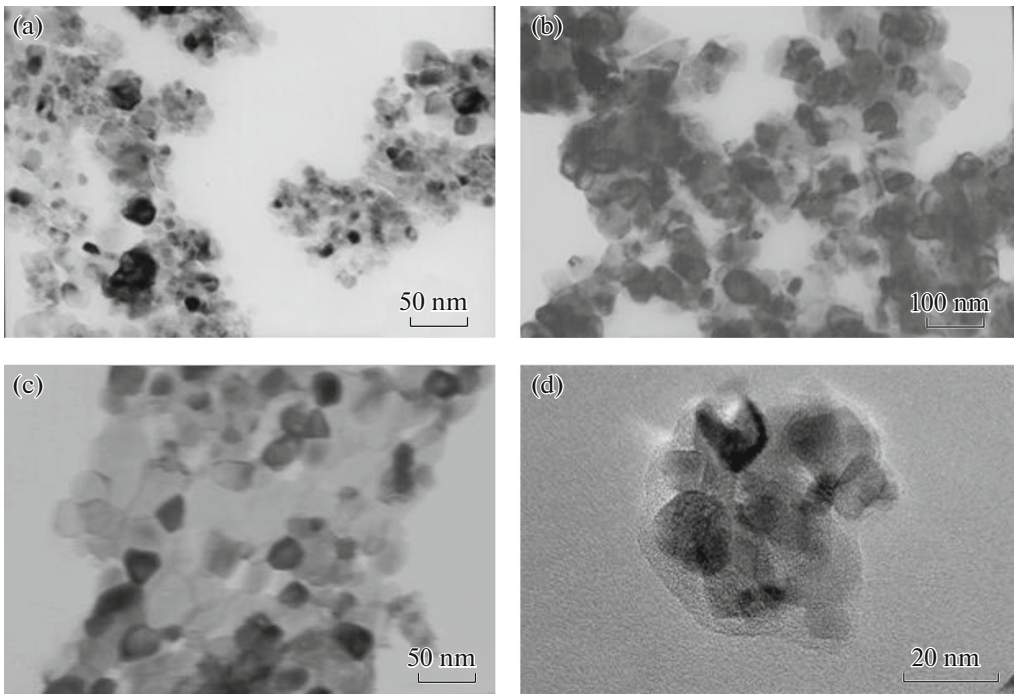

Fig. 2. TEM images of (a) GDC20, (b) Ni–GDC20, and (c) Cu–GDC20 powders obtained by the cellulose precursor method and of (d) initial commercial NiO nanopowder.

particles has a size in the range of 5–15 nm. More than 99.5% of particles are <50 nm in size.

The use of such nanostructured powders for the manufacture of anodes could theoretically be advantageous. However, after screen printing and drying of the layers containing the initial NiO nanopowder, a strong tendency to cracking was observed (Fig. 4a). Defects formed during drying could not be eliminated by any subsequent sintering step. Due to the very poor cohesion and large cracks, such layers cannot be used in practice. It should be noted that this behavior is not observed for other micron and submicron NiO powders used as a component of screen printing pastes. Screen-printing technology for NiO-containing pastes is widely used all over the world for the production of SOFC anodes. Therefore, the observed anomaly was attributed to specific morphological features of the nanosized NiO powder, assessed using TEM in combination with TGA.

TEM revealed that NiO nanoparticles have a core–shell structure (Fig. 2d). Presumably, an amorphous shell up to 5 nm thick is formed due to the absorption of gaseous components from the surrounding atmosphere. Indeed, EDX analysis showed a significantly high oxygen hyperstoichiometry of the nanopowder. The amount of hyperstoichiometric oxygen decreases upon annealing in air and becomes insignificant after heat treatment at temperatures above 500°C. In order to exclude the influence of uncertainties associated with the high error of EDX analysis of light elements, these observations were quantitatively confirmed using TGA. The initial NiO powder was investigated in a flow of air, argon, and a gas mixture with a composition of 4 vol % H_2 and 96 vol % Ar; the mass spectrometric signal was measured by heating in argon. The results are shown in Fig. 5. The mass changes in the atmospheres of air and argon were found to be the same, within the instrumental error. This indicates the absence of any organic adsorbates that could be oxidized in air. Significant weight loss is observed in two temperature ranges. Mass spectrometry data show that

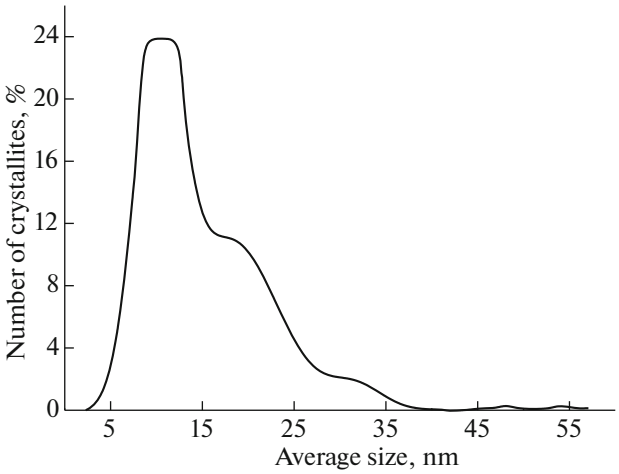

Fig. 3. Particle size distribution of the initial NiO nanopowder, calculated from the TEM results.

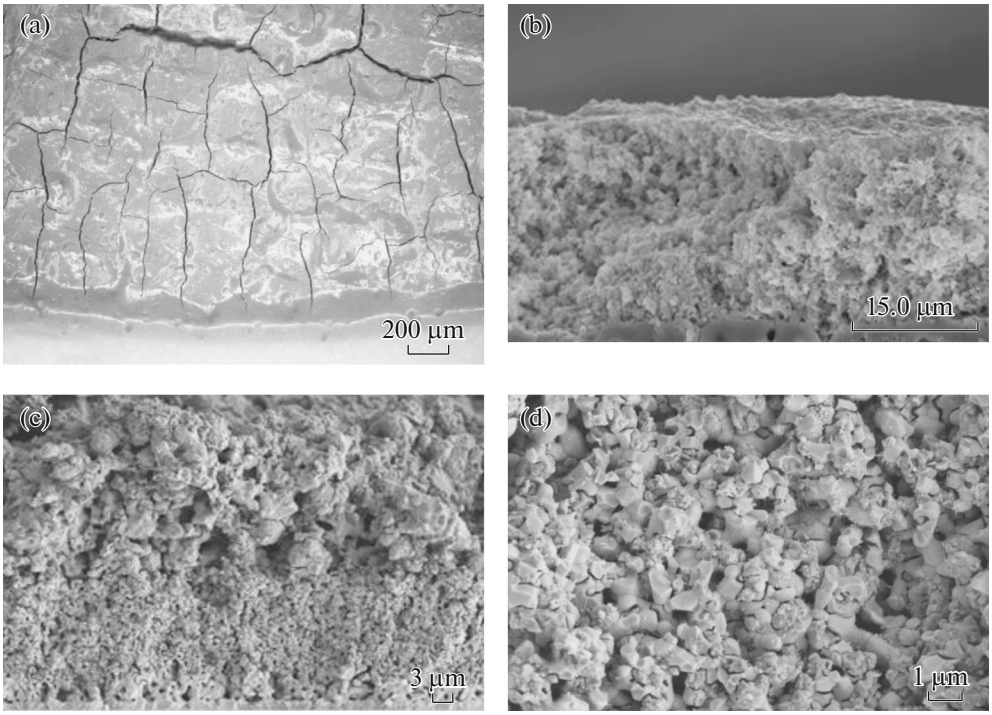

Fig. 4. Functional anode layer applied by screen printing and dried in air at 130°C (a), TEM images of the fracture of an electrochemical cell with a porous anode layer of composition Ni : 8YSZ : GDC20 (50 : 30 : 20 wt %) in contact with solid electrolyte LSGM (b), a model electrochemical cell with a four-layer anode consisting of GDC (thickness 2–4 μm), NiO : GDC20 (40 : 60 wt %, 8–12 μm), NiO : 10Sc1CeSZ (60 : 40 wt %, 15–20 μm) and NiO (<5 μm) sequentially deposited on a commercial solid electrolyte Hionic^{TM} (FuelCellMaterials, USA) (c), and functional layer NiO–GDC20 of the same cell (d).

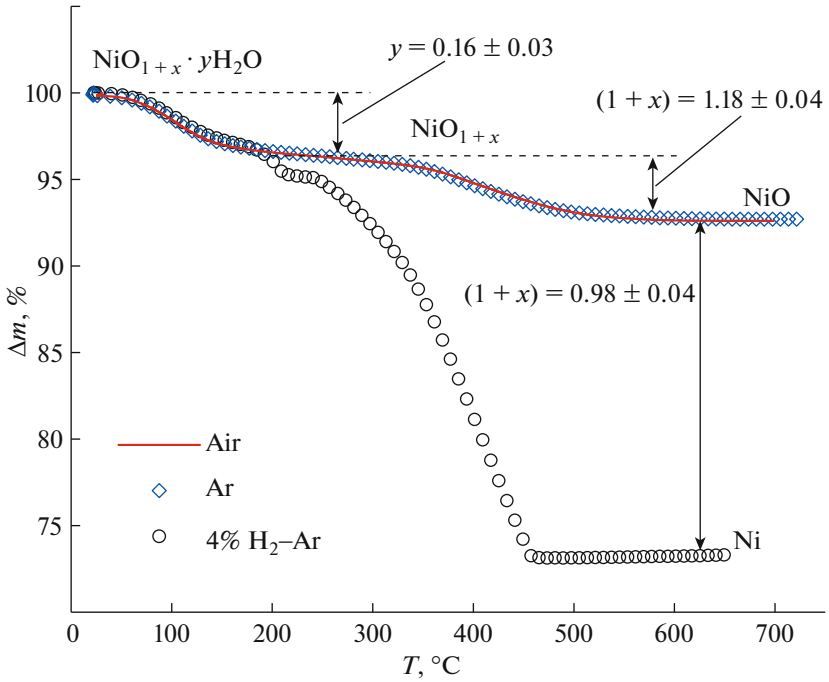

Fig. 5. (Color online) TGA curves of NiO nanopowder in different atmospheres.

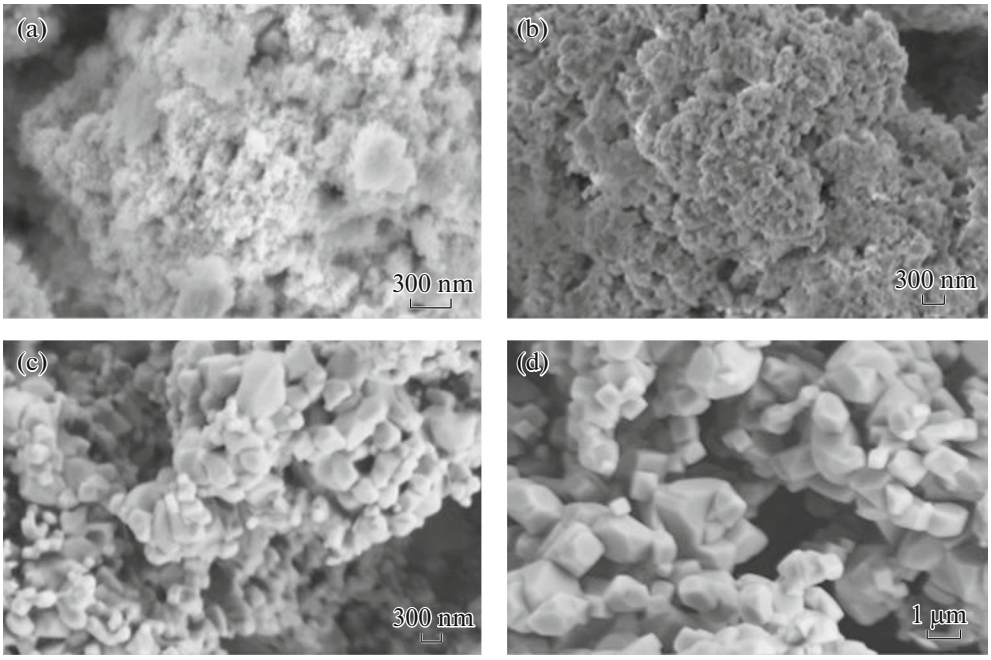

Fig. 6. Morphology of NiO powders annealed in air at 500 (a), 700 (b), 900 (c), and 1100°C (d).

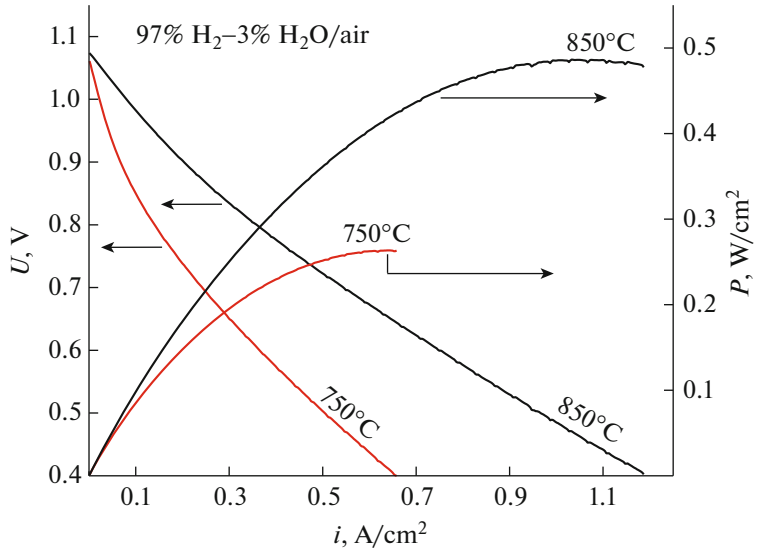

Fig. 7. (Color online) Dependences of voltage and specific power of a model planar SOFC on current density. The model cell consisted of a four-layer anode with layers of GDC20 (thickness 2–4 μm), NiO : GDC20 (40 : 60 wt %, 8–12 μm), NiO : 10Sc1CeSZ (60 : 40 wt %, 15–20 μm), and NiO (<5 μm) and a three-layer cathode with layers GDC20 (2–4 μm), LSM : GDC20 (60 : 40 wt %, 10–15 μm), and LSM (15–20 μm) applied to the commercial solid electrolyte Hionic^{TM} (FuelCellMaterials, USA) and co-fired in air at 1300°C for 2 h.

the first 3.6% mass loss (60–200°C) in the thermogravimetric curves corresponds to dehydration. The calculated content of desorbed water is 0.16±0.03 molecules per formula unit of NiO. The second sharp decrease in mass at 300–600°C is associated with the loss of hyperstoichiometric oxygen. The latter is clearly visible from the peak $m/e = 32$ detected by the mass spectrometer. The total amount of desorbed oxygen corresponds to 0.18±0.04 atoms per formula unit. In the case of H_2-containing atmosphere, desorption of hyperstoichiometric oxygen is combined with the reduction of NiO to metallic nickel. The total oxygen content according to TGA data was calculated relative to the weight of the completely reduced sample.

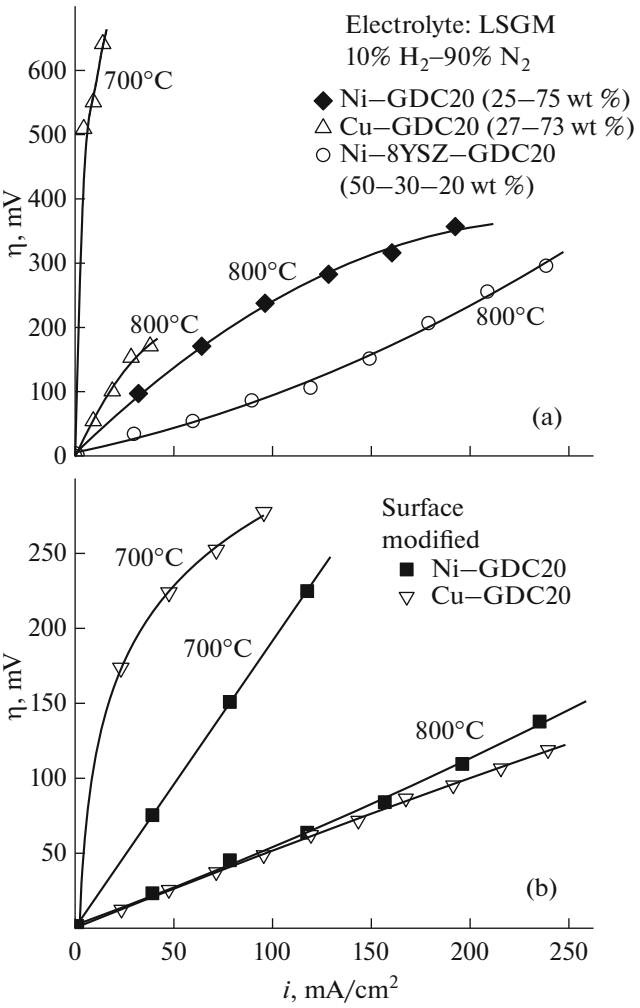

Fig. 8. Anodic overvoltage versus current density for different cermet layers. Surface-modified anodes are obtained by impregnating $CeO_{2-\delta}$ nanoparticles after the first cycle of electrochemical measurements.

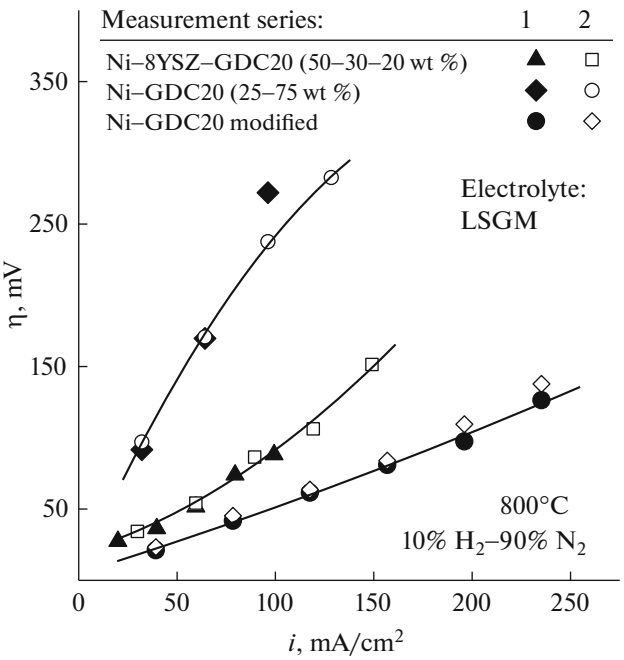

Fig. 9. Overvoltage versus current density for Ni- and Ce-containing cermets, illustrating the reproducibility of the results. The data for the first and second series of measurements correspond to two different anodes, made and modified under identical conditions.

The conclusion about the presence of amorphous surface layers formed during the intercalation of water and oxygen is also confirmed by the preliminary results of Raman spectroscopy. After annealing at 300–500°C, the characteristic Raman peaks of NiO are practically invisible. The first Raman spectrum with well resolved NiO peaks was recorded for a powder annealed at 700°C with adsorbates removed. Preliminary heat treatment at this temperature allows maintaining the submicron particle size (Fig. 6); intensive grain growth begins when heated above 900°C. Therefore, a temperature of 700°C was chosen for the treatment of NiO powder used for the screen printing paste for functional anode layers. The same annealing temperature was chosen to obtain NiO by thermal decomposition of $Ni(NO_3)_2 \cdot 6H_2O$.

Figure 4 shows the microstructures of planar cells, including single and multilayer anodes deposited on solid electrolyte membranes based on doped lanthanum gallate and stabilized zirconia. The functional layers of anodes made of NiO pre-annealed at 700°C have good adhesion to other cell components and a well-developed microstructure with an average particle size of less than 1 μm. This microstructure provides a sufficiently high specific power of model fuel cells (Fig. 7).

At the same time, the growth of the particle size to submicron during the anodes firing shows that further optimization of their electrochemical properties is possible by means of surface modification. Impregnation and chemical etching are promising methods for such modification. Figures 8 and 9 show comparative data on the anodic overpotential obtained before and after the impregnation of $CeO_{2-\delta}$ nanoparticles. The measurements were performed by the three-electrode method in a flow of a humidified mixture of 10% H_2–90% N_2. After electrochemical tests, the selected anodes were surface modified by impregnation with a saturated solution of $Ce(NO_3)_3\ 6H_2O$ in ethanol followed by annealing at 800–1000°C. Then the dependences of overpotential on current were re-measured. The measurement results show that the surface modification by nanoparticles $CeO_{2-\delta}$ leads to a significant reduction in overpotential, of up to 2 to 4 times. This improvement was observed even for the relatively passive Cu-GDC20 cermet anode. Good reproducibility (Fig. 9) and the absence of technological difficulties during impregnation make it possible to count on the introduction of such a technique.

CONCLUSIONS

The pronounced tendency to adsorption of oxygen and water vapor imposes serious restrictions on the use of nanocrystalline NiO for screen printing of SOFC composite anodes. During drying of such layers, cracking and degradation of cohesion occur as a result of heat desorption processes. Most likely, these processes are accompanied by the oxidation of organic components of the paste by hyperstoichiometric oxygen released from NiO_{1+x}. TEM, EDX, and TGA studies revealed significant amounts of hyperstoichiometric oxygen, up to 20–30 at % intercalated into the amorphous surface layers of nanosized NiO particles. This behavior makes it necessary to introduce an additional heat treatment step before the paste is made. It has been shown that annealing at temperatures above 500–600°C is sufficient for the complete removal of adsorbates. Because intensive grain growth begins after heating above 900°C, a pre-treatment temperature of 700°C was chosen as the optimal one. At the same time, the need to form SOFCs at higher temperatures leads to an increase in the particle size to submicron. The electrochemical activity of such anodes can be increased by impregnating nanoparticles onto their surface.

FUNDING

This work was supported by the Russian Science Foundation (grant no. 20-19-00478).

REFERENCES

1. *Solid Oxide Fuels Cells: Facts and Figures: Past Present and Future Perspectives for SOFC Technologies,* Ed. by J. T. S. Irvine and P. Connor (Springer, London, Heidelberg, New York, Dordrecht, 2013).
2. G. Kaur, "SOFC technology: Its working and components," in *Solid Oxide Fuel Cell Components* (Springer, Cham, Switzerland, 2016), p. 79. https://doi.org/10.1007/978-3-319-25598-9_3
3. Z. Shao and M. O. Tade, *Intermediate-Temperature Solid Oxide Fuel Cells: Materials and Applications* (Springer, Berlin, Heidelberg, 2016). https://doi.org/10.1007/978-3-662-52936-2
4. K. Huang and J. B. Goodenough, *Solid Oxide Fuel Cell Technology: Principles, Performance and Operations* (CRC, Woodhead, 2009).
5. *Solid Oxide Fuel Cells: From Materials to System Modeling,* Ed. by M. Ni and T. S. Zhao (Roy. Soc. Chem., London, 2013).
6. E. V. Tsipis and V. V. Kharton, J. Solid State Electrochem. **12**, 1367 (2008).
7. E. V. Tsipis and V. V. Kharton, J. Solid State Electrochem. **15**, 1007 (2011).
8. V. N. Chebotin and M. V. Perfil'ev, *Electrochemistry of Solid Electrolytes* (Khimiya, Moscow, 1978) [in Russian].
9. E. V. Tsipis and V. V. Kharton, J. Solid State Electrochem. **12**, 1039 (2008).
10. E. D. Wachsman and K. T. Lee, Science (Washington, DC, U. S.) **334**, 935 (2011).
11. V. V. Kharton, E. N. Naumovich, V. N. Tikhonovich, et al., J. Power Sources **79**, 242 (1999).
12. V. V. Kharton, E. V. Tsipis, I. P. Marozau, et al., Solid State Ionics **178**, 101 (2007).
13. I. Burmistrov, D. Agarkov, S. Bredikhin, et al., ECS Trans. **57**, 917 (2013).
14. I. N. Burmistrov, D. A. Agarkov, E. V. Korovkin, et al., Russ. J. Electrochem. **53**, 873 (2017).
15. I. Kuritsyna, V. Sinitsyn, A. Melnikov, et al., Solid State Ionics **262**, 349 (2014).